CHAPTER TWELVE

Engineering Oscillating Microtubule Bundles

Timothy Sanchez, Zvonimir Dogic[1]
Department of Physics, Brandeis University, Waltham, Massachusetts, USA
[1]Corresponding author: e-mail address: zdogic@brandeis.edu

Contents

Abstract

From motility of simple protists to determining the handedness of complex vertebrates, highly conserved eukaryotic cilia and flagella are essential for the reproduction and survival of many biological organisms. Despite extensive studies, the exact mechanism by which individual components coordinate their activity to produce ciliary beating patterns remains unknown. We describe a novel approach toward studying ciliary beating. Instead of deconstructing a fully functional organelle from the top-down, we describe a process by which synthetic cilia-like structures are assembled from the bottom-up and we present methods for engineering such structures. We demonstrate how simple mixtures of microtubules, kinesin clusters, and a bundling agent assemble into structures that produce spontaneous oscillations, suggesting that self-organized beating may be a generic feature of internally driven bundles. Synthetic cilia-like structures can be assembled at high density, leading to synchronization and metachronal traveling waves, reminiscent of the waves seen in biological ciliary fields.

Methods in Enzymology, Volume 524
ISSN 0076-6879
http://dx.doi.org/10.1016/B978-0-12-397945-2.00012-3

1. INTRODUCTION

Motile eukaryotic cilia or flagella are highly conserved filamentous organelles that propel cells or move fluid over tissue surfaces by generating reproducible and rhythmic beating patterns (Alberts, Bray, & Lewis, 1994; Bray, 2001). Cilia play an essential role in a variety of biological processes, ranging from the motility in simple protists to mucus clearance in humans. Because of its widespread importance in cell biology, a significant effort spanning many decades has focused on elucidating the rules governing ciliary beating. The extraordinary complexity of cilia, which contain more than 600 different proteins (Pazour, Agrin, Leszyk, & Witman, 2005), presents a particular challenge facing any study of ciliary function, and it has proved difficult to disentangle the exact role of the different constituent proteins. Due to their complexity, most efforts in the past six decades have focused on characterizing biological cilia using top-down approaches, such as structural characterization of intact organelles or deconstructing functional cilia through mutational knockouts of specific structural elements (Dymek & Smith, 2007; Medalia et al., 2002; Pazour et al., 2005; Stolc, Samanta, Tongprasit, & Marshall, 2005). Despite these extensive efforts, the molecular mechanism that controls ciliary beating remains a mystery (Brokaw, 2009; Foster, 2009; Lindemann & Lesich, 2010). Top-down experiments alone have not been able to decipher the properties of these extraordinary organelles.

More recently, a complementary, bottom-up approach aimed at elucidating the mechanisms that drive the spontaneous beating of biological cilia and flagella has emerged. Theoretical coarse-grained models have predicted that ciliary beating may occur due to the self-organization of a few essential components (Brokaw, 1975; Camalet, Julicher, & Prost, 1999; Lindemann & Lesich, 2010). Motivated by such predictions, we have recently demonstrated a minimal *in vitro* system that exhibits spontaneous oscillations. Here, we describe in detail the methods by which to assemble such artificial filamentous bundles that, powered by molecular motors, exhibit periodic beating patterns similar to those of biological cilia. In our model system, beating bundles are assembled in mixtures comprising microtubules (MTs), kinesin clusters, and a depletion agent which holds the MTs together in bundles (Sanchez, Welch, Nicastro, & Dogic, 2011) (Fig. 12.1). Even without the depleting agent, similar mixtures exhibit interesting self-organizing behavior by assembling into aster and vortex-like structures (Leibler, Nedelec, Surrey, & Maggs, 1997; Surrey, Nedelec, Leibler, & Karsenti, 2001).

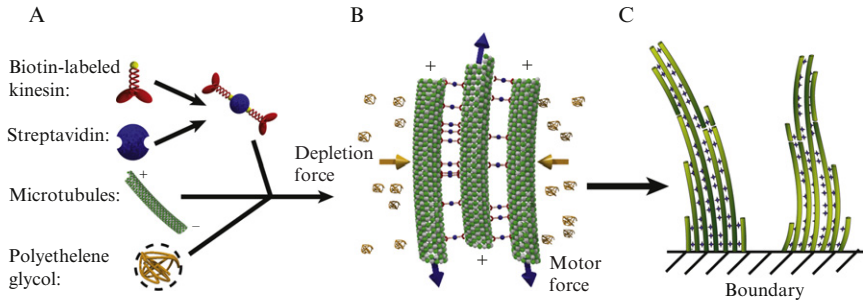

Figure 12.1 Schematic illustration of internally driven bundles that exhibit spontaneous beating. (A) Essential components of active mixtures in which assembly of beating bundles is observed. Biotinylated kinesin motors bound into clusters by a biotin–streptavidin–biotin linkage attach and move along neighboring microtubules. Microtubules are bundled by polyethylene glycol (PEG), a depletion agent. (B) Active MT bundles, internally driven by the motors. MTs are partially inhibited from sliding, which results in spontaneous curvature of the bundles. (C) Once attached at the boundaries of the chamber or at the edge of compressed air bubbles, active bundles can oscillate over many cycles.

In a single cilium, thousands of motors coordinate their activity to produce regular beating patterns. At the next level of hierarchy, within a dense ciliary layer, thousands of cilia coordinate their beating patterns, leading to the formation of traveling metachronal waves. Theoretical models and simulations have predicted that the formation of metachronal waves does not require biochemical regulation, but is a generic result of hydrodynamic interactions between beating cilia (Guirao & Joanny, 2007). Here, we describe methods for assembling densely packed, actively beating bundles that spontaneously synchronize their dynamical behavior to produce collective metachronal waves, similar to what is observed in biological ciliary fields.

The simple *in vitro* system described here has the potential to provide important insights into both the molecular mechanism underlying the beating of isolated eukaryotic cilia and flagella, as well as the principles underlying synchronization in ciliary fields. The ability to tune all relevant parameters will allow for systematic and quantitative tests of theoretical models. In addition to their potential biological relevance, filamentous active bundles with regular and controllable beating patterns could have important nanotechnology applications, ranging from fluid mixing in microfluidic devices to the assembly of autonomously propelled nanostructures (Darnton, Turner, Breuer, & Berg, 2004; den Toonder et al., 2008).

2. PURIFICATION AND PREPARATION OF PROTEINS

2.1. Tubulin purification

The quality and colloidal stability of polymerized MTs greatly affect the behavior of active samples. At room temperature, MTs used in single molecule assays can typically be used for many days if not weeks because they are greatly diluted under experimental conditions. However, when studied at higher concentrations, MTs have a tendency to form cross-links that result in the formation of rigid gel-like structures (Weitz, Lin, Koenderink, & MacKintosh, 2007; Yang, Lin, Kaytanli, Saleh, & Valentine, 2012). The reason for MT cross-linking at high density is not understood. It has been suggested that tubulin monomers which coexist with polymerized MTs denature over time and subsequently stick and cross-link MTs (Daniel Needleman, Havard, personal communication). High-quality polymerized MTs are essential for the successful assembly of synthetic cilia. For this reason, as described below, we have slightly altered previously published MT polymerization protocols in order to minimize the undesirable MT cross-linking. Furthermore, to minimize these effects, we only use MTs that have been polymerized within a day or two.

Tubulin was purified from bovine brain tissue through two cycles of polymerization–depolymerization in high-molarity PIPES buffer (Castoldi & Popova, 2003). Instead of a phosphocellulose column, this protocol uses high-molarity buffer in combination with a differential centrifugation to separate microtubule-associated proteins from MTs. This protocol has several advantages over the traditional chromatography-based protocol. First, it is significantly faster and involves a smaller number of steps, thus making it less likely for an error to occur. Second, after the final centrifugation step, tubulin can be easily resuspended at high concentration before freezing, making it easier to use in subsequent procedures. Third, the fraction of polymerization-competent tubulin is also higher when compared to the previous method. This is probably because a significant fraction of tubulin denatures during the chromatography purification.

At the end of the purification, tubulin was flash-frozen with liquid nitrogen at 7.4 mg/mL in M2B buffer (80 m*M* PIPES, pH 6.8 (w/KOH), 1 m*M* EGTA, 2 m*M* $MgCl_2$) in 500 μL aliquots at −80 °C. Thin-walled tubes (VWR cat. # 53225–647) were used for flash-freezing in order to avoid potentially harmful solvent crystallization. Approximately, 2 kg of brain tissue (nine calf brains) yielded ∼500 mg of tubulin, which was somewhat lower than the yield reported in the original protocol (Castoldi & Popova, 2003).

2.1.1 Tubulin recycling and labeling

Active samples require a small amount of highly concentrated tubulin. 500 μL aliquots of frozen tubulin were thawed, polymerized, and centrifuged to separate fully formed MTs from unpolymerized monomers. The sedimented MT were then depolymerized at low temperature, spun again to separate from aggregates, and then flash-frozen in 5 μL aliquots (final concentration of 13.2 mg/mL). The original recycling procedure polymerizes MTs in the presence of 33% glycerol (Hyman et al., 1991). We found that omitting the glycerol and including 1 m*M* of DTT in this step results in MT gels that are more fluid and have less crosslinking. However, this increase in tubulin quality reduces the yield of the recycling procedure. The use of glycerol resulted in a 75% recovery of the tubulin after recycling. Without glycerol, only 45% of the tubulin was recovered.

For fluorescence microscopy, tubulin was labeled with fluorescent dyes, which were attached to primary amines with a succinimidyl ester linkage (Hyman et al., 1991). We explored the behavior of a few different dyes and found that Alexa-647 (Sigma, A20006) yields the most photostable MTs while also minimizing the amount of undesirable cross-linking. Though we could reproduce our experiments with Alexa-568-labeled tubulin, this dye produced more crosslinked MTs and was not as photostable as Alexa-647. Alexa 488 is not recommended, having produced the dimmest and least photostable MTs.

In the labeling protocol, we again omit glycerol during the first polymerization. However, because labeled monomers constitute only 3% of the monomers in the polymerized MTs, it is not as critical to use highly functional labeled tubulin. Because of this and since the yields are already so low for tubulin labelings, we do use glycerol in the last polymerization of the protocol (final recycling step). With the omission of glycerol in the first step, we obtain between 12% and 15% yield for labeling, which is lower than the commonly reported 25% recovery rate.

An important factor that has a dramatic effect on the yield of recycled tubulin is the formation of air bubbles, particularly during the MT labeling step and the depolymerization step. During labeling and "light vortexing," we noticed that even the shape of the container can cause bubble formation. Vortexing in a cylindrical container produced many bubbles, whereas none occurred in the typical conical eppendorf tube. During depolymerization, we refrained from using a dounce because it can cause large bubbles, especially for small volumes. Instead, we shear the MTs by simply pipetting every 5 min for 30 min, but great care must be taken not to produce bubbles

during this process. The labeled tubulin stock was 7 mg/mL in total tubulin concentration and contained 29% labeled monomers.

2.1.2 MT polymerization

On the morning of an experiment, unlabeled tubulin was copolymerized with the labeled Alexa-647 stock to obtain MTs that contain 3% labeled monomers. The polymerization mixture consisted of the following:
Polymerization mixture

- 1.6 μL glycerol (to 15% of final)
- 0.6 μL GTP (50 m*M*)
- 0.5 μL DTT (20 m*M*)
- 4.5 μL unlabeled tubulin (13.2 mg/mL)
- 0.9 μL of Alexa-labeled tubulin (7 mg/mL)
- 1.7 μL M2B buffer (final tubulin concentration 6.8 mg/mL)

The high viscosity of glycerol makes accurate pipetting difficult, so the liquid is weighed on a scale with submilligram precision. Glycerol promotes nucleation of tubulin polymerization (Kuchnir Fygenson, Flyvbjerg, Sneppen, Libchaber, & Leibler, 1995) and produces a pronounced difference in the quality of the final polymerizations. Polymerizations without glycerol often contain fluorescent aggregates, which can interfere with the bulk dynamics of the final active mixtures. DTT is a reducing agent, which prevents disulfide bonds from forming between the cysteine residues of protein monomers, which can cause protein cross-linking.

Because unpolymerized tubulin quickly denatures, all other components should be mixed first. *Tubulin is thawed immediately before use and subsequently added to the polymerization mixture.* Monomeric tubulin should not be vortexed but rather mixed by gentle pipetting. Once mixed, the solution is transferred immediately to a 37 °C water bath for 30 min. Tubulin is significantly more stable when polymerized; thus denaturation is minimized by polymerizing as quickly as possible. To stabilize the MTs, a 0.5 m*M* taxol dilution (1:1 of M2B to 1 m*M* taxol, dissolved in DMSO) was added to the polymerized MTs, diluting the MT concentration to 6 mg/mL. Adding taxol at once can result in local precipitation of MTs. Therefore, taxol was added in 1/4-volume increments, spaced 7 min apart. The solution was mixed by lightly vortexing in short pulses after each addition of taxol. MTs polymerized in this way were used for up to 2 days.

For our particular tubulin preparation, the above polymerization protocol produced MTs with an average length of 4.8 μm and a standard deviation of 4.1 μm. Length distributions were measured by first preparing a 2000 × dilution

of 6 mg/mL MT stock with antioxidants, trolox, and 2.5% (w/v) of the depletion agent, dextran (MW 500 kDa). Thin chamber samples were prepared by depositing 2 μL of solution onto a clean glass slide and covering it with a clean coverslip. In these samples, dextran causes individual MTs to adsorb onto the glass surface so that the entire contours of the filaments can be imaged. For statistics, a motorized stage (Nikon Eclipse Ti microscope) was used to take hundreds of images, each containing dozens of filaments (Fig. 12.2). The images were analyzed with custom software. The length distribution is a key parameter that critically affects the dynamical behavior of active bundles. For example, reducing the average MT length to below 2 μm leads to entirely different behavior characterized by appearance of macroscopic turbulent-like patters driven by microscopic MT bundle extension, buckling, self-fracture, and healing (Sanchez, Chen, DeCamp, Hyman, & Dogic, 2012). In all likelihood, the length distribution of polymerized MTs is highly dependent on the particular tubulin concentration as well as the characteristics of each purification. For this reason, polymerization protocols should probably be optimized for each tubulin purification in order to obtain MTs with approximately 5-μm average length.

As a final note, many polymerization protocols involve high-speed centrifugation steps, either before polymerization to clarify monomers from protein aggregates or after polymerization to pellet and resuspend the MTs.

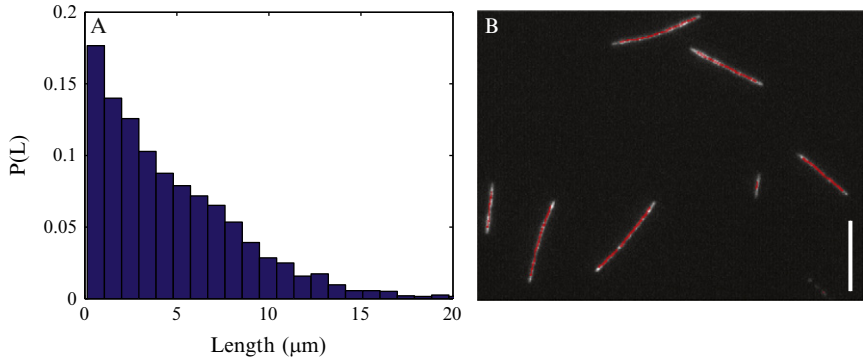

Figure 12.2 Length distribution of polymerized MTs. (A) Normalized probability distribution of MT lengths for the purification and polymerization conditions described in this protocol. MTs have an average length of 4.8 μm and a standard deviation of 4.1 μm. (B) Filament lengths are measured by adsorbing individual filaments onto clean glass surfaces with the depletion agent. Images are taken of thousands of filaments, and then filament contours are identified with custom analysis software. Bar is 10 μm.

We found that omitting these spin steps improved the quality of the polymerized stock, with MTs exhibiting less cross-linking and fewer aggregates.

2.2. Kinesin purification

K401-BIO-6xHIS is the *Drosophila* heavy chain kinesin-1, truncated at residue 401 and fused to the *Escherichia coli* biotin carboxyl carrier protein. The chain also contains a six-histidine tag used for affinity purification with a Nickel column (Berliner, Young, Anderson, Mahtani, & Gelles, 1995; Martin, Fathi, Mitchison, & Gelles, 2010). Briefly, the plasmid that codes K401-BIO-6xHIS was placed transformed into *E. coli,* and the protein expression was induced by IPTG in the presence of free biotin. After growth, bacteria were concentrated, transferred to a lysis buffer, lysed, and centrifuged to obtain a supernatant protein mixture that contains 6xHis-labeled kinesin. The supernatant was then loaded onto a HiTrap nickel column (GE Healthcare 17-0409-01). The histidines on the kinesin chelate the nickel, binding the kinesin onto the column. Subsequently, running an imidazole gradient displaces the histidines, eluting the K401-BIO-6xHis in a distinct peak. The single nickel column purification step differs from the original protocol, which included a stepwise elution of K401-BIO-6xHIS from the nickel column followed by an additional purification step using an ion exchange column. The protein purities of the two methods are comparable; however, the one-step method produces a higher protein yield (several milligrams from 4 L of *E. coli*). Kinesin was suspended in a buffer containing 0.7 mg/mL in 50 m*M* imidazole (pH 6.7), 4 m*M* $MgCl_2$, 2 m*M* DTT, 50 μ*M* ATP, and 36% sucrose, flash-frozen in liquid nitrogen and stored in 8-μL aliquots. When stored at −80 °C, we do not observe any appreciable kinesin degradation for more than 3 years.

2.3. Kinesin–streptavidin complexes

Kinesin–streptavidin complexes were assembled by mixing 7 μL of freshly thawed K401 stock with 0.1 μL of 50 mM DTT and 8 μL of 0.35 mg/mL streptavidin (Invitrogen, S-888), dissolved in M2B. The mixture was allowed to incubate on ice for at least 10 min before diluting with M2B to a final volume of 28 μL.

3. DEPLETION-DRIVEN BUNDLING OF MTs

In axonemes, specialized structures called nexin links cross-link the nine MT doublets (Heuser, Raytchev, Krell, Porter, & Nicastro, 2009). It has been suggested that the nexin link has the ability to bind, dissociate,

and rebind to neighboring MT doublets, thus allowing the two MTs to slide past each other over a significant distance while simultaneously holding their separation to a well-defined value (Minoura, Yagi, & Kamiya, 1999). In synthetic cilia, this function was reconstituted with the inclusion of a non-adsorbing polymer poly(ethylene glycol) which induces MT bundling via the well-characterized depletion mechanism (Fig. 12.3) (Asakura & Oosawa, 1954; Needleman et al., 2004). Furthermore, depleted MTs are still able to slide along each other (Sanchez et al., 2011), thus possibly mimicking the effect of nexin links between MTs in the axoneme.

Experimentally, the depletion mechanism is a highly useful and versatile technique, producing a tunable attractive potential between colloidal particles. The strength of the attraction is tuned by simply altering the PEG concentration. The motor-driven nonequilibrium dynamics are highly dependent on PEG concentration, and synthetic cilia-like beating is only observed within a narrow range of PEG concentrations. Below 0.3%, the bundling potential is not strong enough, and MT-motor suspensions remain

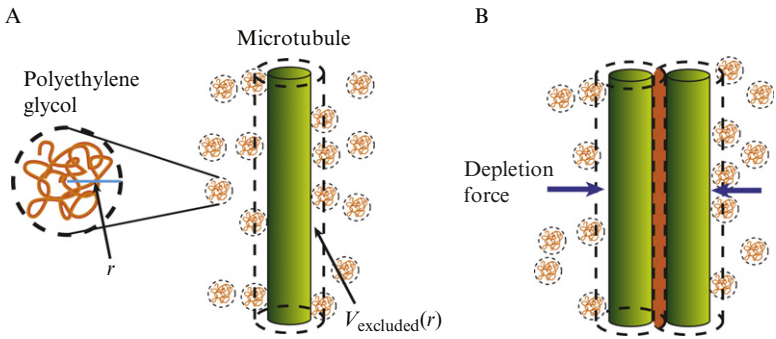

Figure 12.3 Schematic of the depletion effect used to assemble MT bundles. The addition of nonadsorbing polymer induces effective attractive interactions between microtubule filaments. (A) Polyethylene glycol, a nonadsorbing polymer, exerts a uniform osmotic pressure onto an isolated filament. Around each filament is a shell, within which the center of mass of a PEG particle is excluded. The volume of this shell ($V_{excluded}$) is larger than the bare volume of filaments and is indicated with dashed line. (B) When the two filaments are closer to each other than the diameter of the depletion polymers, their excluded volume shells overlap (colored in red) and depletion polymers are prevented from going between the filaments. This leads to a higher polymer concentration outside the filaments than between them, which leads to an imbalance of osmotic pressures and an effective attraction between the filaments. Changing the polymer size and concentration provides a direct means of controlling the range and strength, respectively, of the attractive potential.

disperse and homogenous. Between 0.3% and 0.4% PEG, MTs slowly organize into clusters that have interesting dynamics in their own right, but oscillating bundles rarely occur. PEG concentration between 0.5% and 0.6% seems to be optimal for assembling oscillating bundles. At higher PEG concentrations, bundles form a contractile percolating network, which prevents the formation of free bundle ends, thus precluding bundle beating.

In biological studies, the depletion mechanism is often referred to as "macromolecular crowding" (Ellis, 2001). Having applied this generic technique to other macromolecules like actin filaments, we stress the great potential of the depletion force for engineering customizable interactions in systems with biological components. In addition to serving as a useful analogue for *in vivo* linkers such as nexin, depletion effects due to the crowded environment within the cell may play a larger role than previously expected (Marenduzzo, Finan, & Cook, 2006).

4. GLASS SURFACE TREATMENT, ACRYLAMIDE COATING, AND FLOW CELL CONSTRUCTION

In a conventional biofilament gliding assay, it is possible to obtain interesting dynamics that bear some resemblance to ciliary beating by simply clamping a filament at its leading front (Bourdieu, Duke, & Elowitz, 1995). In order to ensure that beating of synthetic MT bundles is driven by internal motor-driven forces alone and not by surface-bound kinesin, we have developed protocols that inhibit nonspecific binding of kinesin to glass surfaces. To accomplish this, glass surfaces are coated with an acrylamide polymer brush (Lau, Prasad, & Dogic, 2009). When polymerized off the surface of the clean glass, polyacrylamide forms a repulsive polymer brush that must be compressed in order for proteins such as a kinesin to approach the surface. This compression comes at an entropic cost. Thus, the brush provides a mechanism that prevents a wide variety of proteins and other nanometer-sized structures from sticking to the surface.

Glass cleaning

1. Immerse slides/coverslips in Millipore pure water with 0.5% Hellmanex detergent (Sigma—61257 FLUKA)
2. Microwave container until almost boiling and sonicate for 5 min
3. Rinse with pure water at least seven times, fill with ethanol, and sonicate for 5 min
4. Rinse with pure water, fill with 0.1 *M* KOH and sonicate for 5 min
5. Rinse and store in pure water

Acrylamide coating

1. Prepare a solution of 2% (w/v) acrylamide (Sigma, A8887) in pure water and place solution under vacuum for 15–30 min to remove any dissolved oxygen which inhibits acrylamide polymerization
2. Prepare a silane-coupling solution immediately before use
   - 98.5% ethanol
   - 1% acetic acid
   - 0.5% 3-(Trimethoxysilyl)propylmethacrylate (Acros Organics, 216551000)
3. Immerse cleaned slides/coverslips in silane-coupling solution for 15 min
4. Rinse slides and empty
5. Transfer 2% acrylamide solution to stirring platform and begin stirring
6. Add 35 μL of TEMED (Sigma, T9281) per 100 mL of acrylamide solution
7. Add 70 mg of ammonium persulfate (Sigma, A3678) per 100 mL of acrylamide solution
8. As soon as components are mixed, pour acrylamide solution into slide/coverslip containers
9. Leave for at least 2 h in order for acrylamide to polymerize

Slides/coverslips can be stored in the final polymerized acrylamide solution for a few weeks and should be covered to avoid contamination from dust. They should be rinsed with pure water and dried with clean air before use. Using acrylamide-coated glass slides and coverslips, 3-mm-wide flow chambers were constructed of thickness ranging from 10 to 90 μm. 10- and 30-μm chambers could be constructed using double-sided tape from Nitto Denko Corporation, while 90-μm chambers were constructed with conventional Scott double-sided tape.

Controls were performed to verify that neither MTs nor kinesin were binding to acrylamide-coated surfaces. First, in the presence of dextran (500,000 MW) around 0.5% (w/v), MTs adsorb on clean glass surfaces; however, in the presence of acrylamide, dextran concentrations can be as high as 2% without inducing evidence of MT adsorption. To test for motor adsorption, side-by-side gliding motility samples (Scholey, 1993) were prepared in clean glass and acrylamide-coated flow chambers. In our assay, motors are deliberately deposited on the surfaces by sequentially flowing biotin-BSA, streptavidin, and biotinylated kinesin. In a final step, MTs are flowed in. If motors are properly bound to the surface, MTs bind and glide along the surface. In the comparison experiments, we obtained MT motility on cleaned glass surface, but no surface binding or motility for the acrylamide-coated slides. Finally, in standard oscillating bundle samples, we

observe three-dimensional, "propeller" beating patterns, which cannot be due to surface interactions. We conclude, therefore, that the oscillations are primarily driven by internal motor forces.

Poly(acrylamide)-coated slides might have a wider use in microscopy, where a frequent challenge encountered is preparing surface treatments that suppress nonspecific sticking of proteins. Among others, traditional methods include passivating surfaces with BSA, surfactants, agarose, and poly(ethylene glycol) that is either attached through silane or an amino reactive group (Nédélec & Surrey, 2001). When our samples are evaluated for nonspecific sticking, poly(acrylamide)-coated surfaces are superior to these other methods. For this reason they might have a wide applicability in instances where nonsticking surfaces are an essential requirement for optical microscopy. It should be noted, however, that the effectiveness of the acrylamide surfaces is not universal for all macromolecules or proteins.

5. ACTIVE MT BUNDLE SAMPLES

The components required for assembly of self-oscillating bundles including MTs, kinesin clusters, and a depletion agent were mixed in an eppendorf tube (Fig. 12.1). In addition, our samples contained (1) an oxygen scavenging system in order to reduce photobleaching and (2) an ATP regeneration system that quickly recycles the ADP produced by motile kinesins back into ATP, thus maintaining a constant ATP concentration for the duration of each experiment. For convenience, several initial mixtures were prepared separately and then combined into the final solution. These components were dissolved and frozen in M2B buffer and thawed freshly for use on the day of experiments.

Taxol–$MgCl_2$ solution: a mixture of taxol and high-salt M2B to stabilize the MTs and to raise the $MgCl_2$, in accordance with previous protocols for MT/kinesin mixtures (Leibler et al., 1997).

- 80 m*M* PIPES, pH 6.8 (w/KOH)
- 69 m*M* $MgCl_2$
- 1 m*M* EGTA
- 130 μ*M* taxol

Next, we included antioxidant stock solutions and trolox (Sigma, 238813) to avoid photobleaching during fluorescence imaging. Antioxidant components are frozen in M2B.

Antioxidant solution 1 (AO1)

- 15 mg/mL glucose
- 25 m*M* DTT

Antioxidant solution 2 (AO2)

- 10 mg/mL glucose oxidase (Sigma G2133)
- 1.75 mg/mL catalase (Sigma C40)

ATP-regenerating components included the enzyme mixture PK/LDH (Sigma, P-0294) and phosphoenol pyruvate (PEP, VWR AAB20358-06), which is the fuel source used by the PK/LDH to recycle ADP back into ATP. All components were mixed in large volumes without MTs to reduce pipetting inaccuracies while not wasting valuable tubulin.

Active premixture

- 1.3 μL AO1
- 1.3 μL AO2
- 1.7 μL ATP (50 m*M*)
- 1.7 μL PK/LDH
- 2.9 μL taxol–$MgCl_2$ solution
- 6 μL trolox (20 m*M*)
- 8 μL PEP (200 m*M*)
- *X* μL kinesin–streptavidin solution
- *Y* μL PEG (6 % w/v in M2B)
- $(27.1 - X - Y)$ μL M2B buffer

The total volume of the active premixture is 50 μL. Using this protocol it is easy to tune the two most important parameters that affect the behavior of the active system: concentration of motor clusters and depleting agents. Most of our samples were prepared with 4 μL of kinesin–streptavidin and either 5 or 6 μL of PEG. To prepare the final active mixture, 5 μL of the active premixture was mixed with 1 μL of the 6 mg/mL MT stock, resulting in a final MT concentration of 1 mg/mL.

We have observed spontaneous assembly of actively beating bundles in two different experimental conditions. Bundles can assemble either at the interfaces of air bubbles that are frequently dispersed throughout the flow chamber or they can attach to the edge of the spacer used for assembly of flow chambers. In our experience, the first method is significantly more robust and almost always leads to actively beating bundles. Its drawback is that the density of beating bundles is usually quite high, thus making it more difficult to study beating of isolated structures. As bubble-bound bundles are also shorter, the latter method of bundle assembly is necessary for studying longer bundles. Moving forward, a significant challenge is to design more robust methods that will lead to assembly of oscillating bundles with well-defined separation, number of filaments, and contour length.

5.1. Self-assembly of active bundles at the air–water interface of air bubbles

Final active mixture was flowed directly into the flow chambers and immediately observed with fluorescence microscopy. The flow frequently caused the formation of air bubbles within the chamber. These bubbles, typically between 50 and 300 μm in diameter, and entrapped within a 10-μm-thick flow chamber, serve as efficient attachment sites for assembly of active bundles. After introducing active mixtures, samples were allowed to develop for 45 min. During this time, bulk MT networks contract away from bubble edges, often trapping between the air bubbles and the glass many bundles that spontaneously start exhibiting 3D beating patterns. Bundles formed in this way are typically shorter ($\sim$10 μm) and thinner than bundles that are assembled at the chamber's edge. Consequently, it is likely that the majority of the MTs in these bundles are attached at the base, largely inhibiting internal dynamic rearrangement of MTs and producing more stable beating patterns.

An alternative method of assembling bubble-bound bundles can be performed by flowing out the bulk MTs after some MTs have adhered to bubble edges ($\sim$20 min), replacing the suspension with active premixture. As the MT network is flowed out, thick swaths of MTs are forced against bubbles. Within these swaths, we once again see the development of bundles that oscillate and synchronize their beating as excess MTs in these swaths diffuse into the empty bulk (Fig. 12.4). This configuration serves as an important control by demonstrating that interaction with background MTs is not required for oscillations. An open-ended flow cell also makes it possible to dynamically change other suspension conditions, thus providing a means of studying how MT beating depends on parameters such as ATP or kinesin cluster concentrations.

5.2. Self-assembly of active bundles at the edge of a flow cell

In the same samples that produce bubble-bound bundles, we also observe the assembly of oscillating bundles at the edge of the flow cell, albeit at a lower density. After initial injection into the flow cell, samples are allowed to develop for tens of minutes before oscillating bundles can be observed. In the initial stages, the bulk MT network contracts, pulling away from the edges of the chamber (Fig. 12.5). While most MTs are pulled away with the contracting bulk network, some MT bundles adhere to the tape at the boundary of the chamber. In these bundles, we see two types of behavior. Some bundles may oscillate once or twice but soon become static. Alternatively, in other regions, tape-bound MT bundles undergo sustained

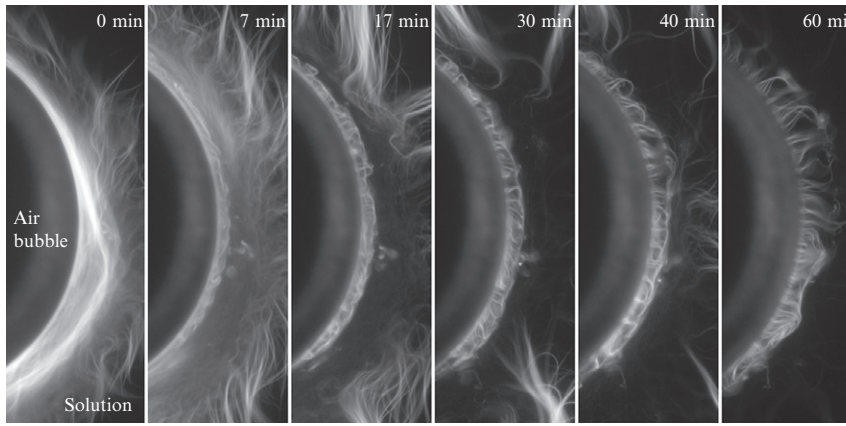

Figure 12.4 Illustration of a robust method used for assembling an active bundle array along the edge of a compressed air bubble. An active mixture containing MTs is replaced with a solution containing all components except MTs. The flow compresses swaths of MTs against air bubbles, but active forces and diffusion soon cause the swaths to disperse into the now-empty bulk of the solution. A dense and dynamic array of MT bundles remaining attached to the interface oscillates without interference from the background MTs. Bar is 40 μm.

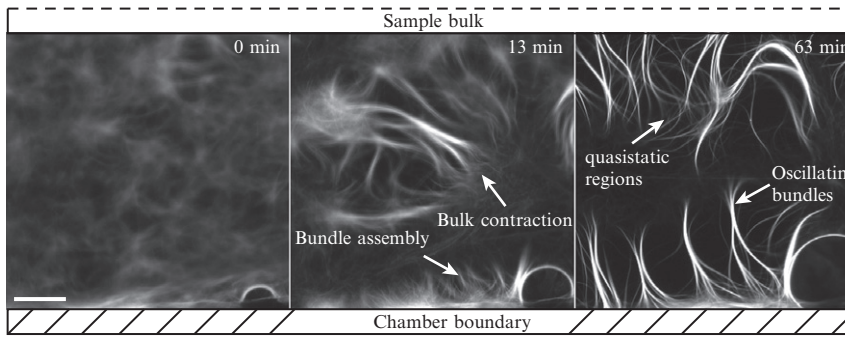

Figure 12.5 Time series illustrating development of active microtubule network. Oscillating bundles self-organize within a highly heterogeneous process, which involves contraction of the bulk MT network away from the edge of the chamber. During the initial stages of network bulk contraction and MT bundling, some bundles assemble at the boundary of the chamber. A certain fraction of these bundles exhibits sustained oscillations. Bar is 50 μm.

oscillations for periods longer than an hour (Fig. 12.6). In a few cases, even quasistatic clusters in the bulk MT network can serve as a basal anchoring point for oscillating bundles.

With subtle differences within the same sample accounting for such drastically different behavior, one of the main challenges is to characterize the

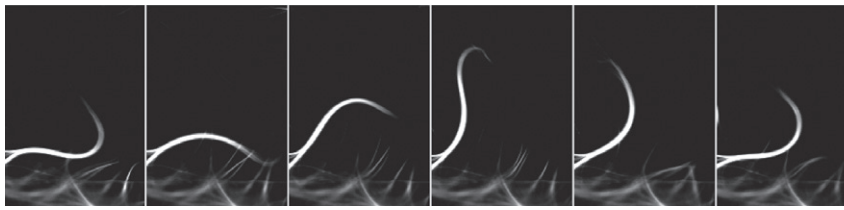

Figure 12.6 Internally driven beating of an isolated active microtubule bundle. Bundle is mounted at the lower tape boundary of the flow cell chamber, where other MT bundle fragments can be seen, and protrudes into the bulk of the sample. Time series depicts one full beat cycle. Time interval between frames is 2.25 min, and scale bar is 40 μm.

differences between beating and nonbeating bundles. Several aspects of the internal structure of these tape-bound bundles are yet to be characterized, but we can surmise several things from the experimental observations. Unlike bundles assembled at an air–solvent interface which are approximately 10 μm long, tape-bound bundles are up to 100 μm long. We know that bundles are staggered composites of overlapping MTs because the total bundle length is significantly larger than any individual MTs observed. That is, MTs within tape-bound bundles are not all attached at the same basal point.

The motor-dependent interfilament sliding depends on their relative polarity. Motors induce sliding between filaments of opposite polarity, while no sliding occurs for filaments with the same polarity (Hentrich & Surrey, 2010). We hypothesize that active bundles contain MTs with mixed polarity and that oscillatory beating is driven by the motor-induced interfilament sliding between neighboring antiparallel MTs. In contrast, nonbeating bundles are assembled from MTs that are locally polarity sorted.

Without any restriction, MTs would quickly slide off each other and polarity sort, but that is not observed in experiments. We investigated the internal dynamics of MTs within bundles by labeling a small fraction of MTs with a different fluorophore. We found that individual MTs do translate within the bundle, but that their movement is much slower than the movement of a freely sliding MT in a gliding assay. Figure 12.7 shows one measurement where an MT slides at 13 nm/s, compared with the free sliding velocity of 600 nm found in traditional gliding assays (Howard, Hudspeth, & Vale, 1989).

The impeded MT movement indicates the presence of interactions between MTs that resist sliding. This may be due to an intermolecular friction induced by the adhesive depletion forces (Sanchez et al., 2011) or due to motor cross-links. In either case, the restrictive interaction transforms the linear sliding motion into local bending, which is essential for the self-organization

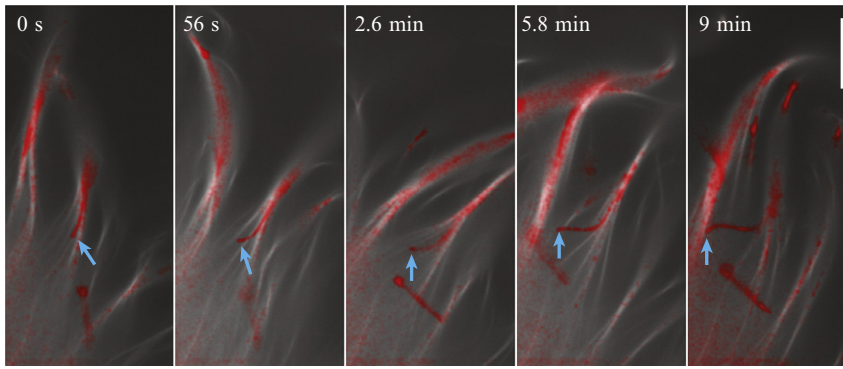

Figure 12.7 Internal rearrangement of MTs within an active bundle. A small fraction of MTs are labeled with Alexa-568 (pseudo colored in red) to visualize individual MTs within active bundles. Most MTs comprising the bundles are labeled with Alexa-647 (appearing in gray). In this time series, an individual MT, indicated with a blue arrow, slides out of the oscillating bundle due to motor forces. The sliding speed, however, is 13 nm/s—almost two orders of magnitude slower than the velocity of a freely sliding MT being moved by kinesins. Impeded sliding is necessary for the generation of bundle curvature. Bar is 10 μm.

of large-scale beating patterns. With internal MT rearrangement though, if there is no influx of MTs into a bundle, the bundles will eventually polarity sort, which results in cessation of interfilament sliding and overall bundle oscillations.

5.3. Bundle synchronization and the emergence of metachronal waves

Within a single cilium, the activity of hundreds of motors spontaneously synchronizes to produce oscillations. At the next level of hierarchy, hundreds of cilia within a dense field synchronize their beating to produce traveling metachronal waves (Afzelius, 2004; Aiello & Sleigh, 1972). This is observed in a diversity of systems from microorganisms such as *Opalina ranarum*, which employs this mechanism to swim, to the human trachea which is covered with dense ciliary fields that efficiently move debris out of the lungs. Beyond the predictions that bundles can spontaneously oscillate due to the coordination of internal motors, other theoretical models have also focused on the interactions between actively oscillating bundles, predicting bundle synchronization and the self-organization of collective beating patterns (Gueron & Levit-Gurevich, 1999). Of particular interest in these theoretical studies is the emergence of propagating metachronal waves in the beating phase of

arrays of oscillating bundles. In these models, traveling waves arise merely from hydrodynamic and/or steric coupling between neighboring cilia (Guirao & Joanny, 2007).

Previous experiments have observed synchronization of autonomous oscillators, which are driven by external fields (Vilfan et al., 2010). In our experiments, however, we observed synchronization of bundles that are *internally* driven, as are cilia. This occurs either in closely spaced bundles bound to the edge of the chamber or more frequently along the edge of the air bubbles described previously. Furthermore, the specific pattern of metachronal waves was also observed to spontaneously emerge in bubble-bound bundle arrays due to the high density of bundles at this interface. The interactions between bundles are not simply hydrodynamic, but also steric and sticky, suggesting that the self-organized beating patterns may be a generic feature of oscillating bundle arrays. These beating patterns were characterized by measuring the intensity profile along the bubble edge, revealing a propagating density profile with clear spatial and temporal wavelengths (Sanchez et al., 2011). Notably, the periodicity of many oscillators acting together is more stable and ordered than that of an isolated bundle.

6. PROTOCOL QUALIFICATIONS AND OUTLOOK

The protocols described within this chapter represent a successful attempt to produce biomimetic oscillating bundles from purely biological components. As such, they present an opportunity to advance our efforts to understand the microscopic mechanism that drives ciliary beating. However, we emphasize that the described protocols are preliminary and are being further developed in our laboratory. For this reason, they should not be taken as the definitive or final method for assembling oscillating bundles. There is space for significant optimization and improvement. This will be necessary if we are to ask more specific questions about the microscopic mechanism behind ciliary beating or make progress toward possible applications such as the engineering of microscopic swimmers.

The most immediate challenge is the inherent polydispersity of bundle assembly as well as their attachment at the base that cannot yet be tuned or controlled in a systematic way. A more controlled method is needed to assemble MT bundles on specific substrates with well-defined, reproducible length; number of filaments; and lateral spacing. For applications, the beating frequency of the bundles must also be increased. The experimental method described here represents an important starting point for such further developments in the field.

ACKNOWLEDGMENTS

We are grateful to J. Chung and J. Gelles for their help in purification of microtubules and kinesin and for the gift of K401-BIO-6xHis. This work was supported by funding from the W. M. Keck Foundation, National Science Foundation (DMR-MRSEC-0820492), and National Institutes of Health (5K25GM85613). We acknowledge the use of MRSEC Optical Microscopy facilities.

REFERENCES

Afzelius, B. A. (2004). Cilia-related diseases. *The Journal of Pathology*, *204*, 470–477.

Aiello, E., & Sleigh, M. A. (1972). The metachronal wave of lateral cilia of *Mytilus edulis*. *The Journal of Cell Biology*, *54*, 493–506.

Alberts, B., Bray, D., & Lewis, J. (1994). Microtubules. In *Molecular biology of the cell*. (3rd ed.). New York: Garland Publishing Inc.

Asakura, S., & Oosawa, F. (1954). On interaction between 2 bodies immersed in a solution of macromolecules. *The Journal of Chemical Physics*, *22*, 1255–1256.

Berliner, E., Young, E. C., Anderson, K., Mahtani, H. K., & Gelles, J. (1995). Failure of a single-headed kinesin to track parallel to microtubule protofilaments. *Nature*, *373*, 718–721.

Bourdieu, L., Duke, T., & Elowitz, M. (1995). Spiral defects in motility assays: A measure of motor protein force. *Physical Review*, *75*, 176–179.

Bray, D. (2001). *Cell movements: From molecules to motility*. New York: Garland Publishing.

Brokaw, C. J. (1975). Molecular mechanism for oscillation in flagella and muscle. *Proceedings of the National Academy of Sciences of the United States of America*, *72*, 3102–3106.

Brokaw, C. J. (2009). Thinking about flagellar oscillation. *Cell Motility and the Cytoskeleton*, *66*, 425–436.

Camalet, S., Julicher, F., & Prost, J. (1999). Self-organized beating and swimming of internally driven filaments. *Physical Review Letters*, *82*, 1590–1593.

Castoldi, M., & Popova, A. V. (2003). Purification of brain tubulin through two cycles of polymerization-depolymerization in a high-molarity buffer. *Protein Expression and Purification*, *32*, 83–88.

Darnton, N., Turner, L., Breuer, K., & Berg, H. C. (2004). Moving fluid with bacterial carpets. *Biophysical Journal*, *86*, 1863–1870.

den Toonder, J., Bos, F., Broer, D., Filippini, L., Gillies, M., de Goede, J., et al. (2008). Artificial cilia for active micro-fluidic mixing. *Lab on a Chip*, *8*, 533–541.

Dymek, E. E., & Smith, E. F. (2007). A conserved CaM- and radial spoke associated complex mediates regulation of flagellar dynein activity. *The Journal of Cell Biology*, *179*, 515–526.

Ellis, R. J. (2001). Macromolecular crowding: Obvious but underappreciated. *Trends in Biochemical Sciences*, *26*, 597–604.

Foster, K. W. (2009). Analysis of the ciliary/flagellar beating of Chlamydomonas. *Methods in Cell Biology*, *91*, 173–239.

Gueron, S., & Levit-Gurevich, K. (1999). Energetic considerations of ciliary beating and the advantage of metachronal coordination. *Proceedings of the National Academy of Sciences of the United States of America*, *96*, 12240–12245.

Guirao, B., & Joanny, J. F. (2007). Spontaneous creation of macroscopic flow and metachronal waves in an array of cilia. *Biophysical Journal*, *92*, 1900–1917.

Hentrich, C., & Surrey, T. (2010). Microtubule organization by the antagonistic mitotic motors kinesin-5 and kinesin-14. *The Journal of Cell Biology*, *189*, 465–480.

Heuser, T., Raytchev, M., Krell, J., Porter, M. E., & Nicastro, D. (2009). The dynein regulatory complex is the nexin link and a major regulatory node in cilia and flagella. *The Journal of Cell Biology*, *187*, 921–933.

Howard, J., Hudspeth, A. J., & Vale, R. D. (1989). Movement of microtubules by single kinesin molecules. *Nature*, *342*, 154–158.

Hyman, A., Drechsel, D., Kellogg, D., Salser, S., Sawin, K., Steffen, P., et al. (1991). Preparation of modified tubulins. *Methods in Enzymology*, *196*, 478–485.

Kuchnir Fygenson, D., Flyvbjerg, H., Sneppen, K., Libchaber, A., & Leibler, S. (1995). Spontaneous nucleation of microtubules. *Physical Rev. E*, *51*, 5058–5063.

Lau, A. W. C., Prasad, A., & Dogic, Z. (2009). Condensation of isolated semi-flexible filaments driven by depletion interactions. *Europhysics Letters*, *87*, 48006.

Leibler, S., Nedelec, F. J., Surrey, T., & Maggs, A. C. (1997). Self-organization of microtubules and motors. *Nature*, *389*, 305–308.

Lindemann, C. B., & Lesich, K. A. (2010). Flagellar and ciliary beating: The proven and the possible. *Journal of Cell Science*, *123*, 519–528.

Marenduzzo, D., Finan, K., & Cook, P. R. (2006). The depletion attraction: An underappreciated force driving cellular organization. *The Journal of Cell Biology*, *175*, 681–686.

Martin, D. S., Fathi, R., Mitchison, T. J., & Gelles, J. (2010). FRET measurements of kinesin neck orientation reveal a structural basis for processivity and asymmetry. *Proceedings of the National Academy of Sciences of the United States of America*, *107*, 5453–5458.

Medalia, O., Weber, I., Frangakis, A. S., Nicastro, D., Gerisch, G., & Baumeister, W. (2002). Macromolecular architecture in eukaryotic cells visualized by cryoelectron tomography. *Science (New York)*, *298*, 1209–1213.

Minoura, I., Yagi, T., & Kamiya, R. (1999). Direct measurement of inter-doublet elasticity in flagellar axonemes. *Cell Structure and Function*, *24*, 27–33.

Nédélec, F., & Surrey, T. (2001). Assaying spatial organization of microtubules by kinesin motors. *Methods in Molecular Biology*, *164*, 213–222.

Needleman, D. J., Ojeda-Lopez, M. A., Raviv, U., Ewert, K., Jones, J. B., Miller, H. P., et al. (2004). Synchrotron X-ray diffraction study of microtubules buckling and bundling under osmotic stress: A probe of interprotofilament interactions. *Physical Review Letters*, *93*, 198104.

Pazour, G. J., Agrin, N., Leszyk, J., & Witman, G. B. (2005). Proteomic analysis of a eukaryotic cilium. *The Journal of Cell Biology*, *170*, 103–113.

Sanchez, T., Chen, D., DeCamp, S., Hyman, M., & Dogic, Z. (2012). Spontaneous motion in hierarchically assembled active matter. *Nature*, *491*, 431–434.

Sanchez, T., Welch, D., Nicastro, D., & Dogic, Z. (2011). Cilia-like beating of active microtubule bundles. *Science*, *333*, 456–459.

Scholey, J. M. (1993). Motility assays for motor proteins. *Methods in Cell Biology, 39*, San Diego CA: Academic Press.

Stolc, V., Samanta, M. P., Tongprasit, W., & Marshall, W. F. (2005). Genome-wide transcriptional analysis of flagellar regeneration in *Chlamydomonas reinhardtii* identifies orthologs of ciliary disease genes. *Proceedings of the National Academy of Sciences of the United States of America*, *102*, 3703–3707.

Surrey, T., Nedelec, F., Leibler, S., & Karsenti, E. (2001). Physical properties determining self-organization of motors and microtubules. *Science*, *292*, 1167–1171.

Vilfan, M., Potocnik, A., Kavcic, B., Osterman, N., Poberaj, I., Vilfan, A., et al. (2010). Self-assembled artificial cilia. *Proceedings of the National Academy of Sciences of the United States of America*, *107*, 1844–1847.

Weitz, D. A., Lin, Y. C., Koenderink, G. H., & MacKintosh, F. C. (2007). Viscoelastic properties of microtubule networks. *Macromolecules*, *40*, 7714–7720.

Yang, Y., Lin, J., Kaytanli, B., Saleh, O. A., & Valentine, M. T. (2012). Direct correlation between creep compliance and deformation in entangled and sparsely crosslinked microtubule networks. *Soft Matter*, *8*, 1776.